The Astrophysical Journal, 727:91 (11pp), 2011 February 1 doi:10.1088/0004-637X/727/2/91

FLUORESCENCE EXCITATION MODELS OF AMMONIA AND AMIDOGEN RADICAL (NH_2) IN COMETS: APPLICATION TO COMET C/2004 Q2 (MACHHOLZ)

Hideyo Kawakita[1] and Michael J. Mumma[2]
[1] Department of Physics, Faculty of Science, Kyoto Sangyo University, Motoyama, Kamigamo, Kita-ku, Kyoto 603-8555, Japan; kawakthd@cc.kyoto-su.ac.jp
[2] Solar System Exploration Division, Mailstop 690.3, NASA Godard Space Flight Center, Greenbelt, MD 20771, USA
Received 2010 June 14; accepted 2010 October 16; published 2011 January 10

ABSTRACT

Ammonia is a major reservoir of nitrogen atoms in cometary materials. However, detections of ammonia in comets are rare, with several achieved at radio wavelengths. A few more detections were obtained through near-infrared observations (around the 3 μm wavelength region), but moderate relative velocity shifts are required to separate emission lines of cometary ammonia from telluric absorption lines in the 3 μm wavelength region. On the other hand, the amidogen radical (NH_2—a photodissociation product of ammonia in the coma) also shows rovibrational emission lines in the 3 μm wavelength region. Thus, gas production rates for ammonia can be determined from the rovibrational emission lines of ammonia (directly) and amidogen radical (indirectly) simultaneously in the near-infrared. In this article, we present new fluorescence excitation models for cometary ammonia and amidogen radical in the near-infrared, and we apply these models to the near-infrared high-dispersion spectra of comet C/2004 Q2 (Machholz) to determine the mixing ratio of ammonia to water in the comet. Based on direct detection of NH_3 lines, the mixing ratio of NH_3/H_2O is 0.46% ± 0.03% in C/2004 Q2 (Machholz), in agreement with other results. The mixing ratio of ammonia determined from the NH_2 observations (0.31%–0.79%) is consistent but has relatively larger error, owing to uncertainty in the photodissociation rates of ammonia. At the present level of accuracy, we confirm that NH_3 could be the sole parent of NH_2 in this comet.

Key words: comets: general – comets: individual (C/2004 Q2 (Machholz)) – line: formation – line: identification

Online-only material: color figures, machine-readable tables

1. INTRODUCTION

Ammonia (NH_3) is a major reservoir of nitrogen atoms in cometary ice. It was first detected in mass spectra of comet Halley acquired in situ by the spacecraft "*Giotto*" (Allen et al. 1987; Meier et al. 1994). Subsequent ground-based searches in comets have been adversely affected by low spatial resolution at radio wavelengths and by telluric absorption at infrared wavelengths.

Ground-based radio observers have searched for inversion transitions of ammonia (near 24 GHz) in many comets, but these lines were firmly detected only in comets C/1996 B2 (Hyakutake) and C/1995 O1 (Hale-Bopp) (Palmer et al. 1996; Bird et al. 1997; Hirota et al. 1999). Bird et al. (2002) also reported a marginal detection of ammonia in comet 153P/Ikeya-Zhang. The radio beam size near 24 GHz is usually larger than the region where ammonia molecules exist in the coma (about 5000 km at 1 AU from the Sun), and the resulting beam dilution decreases the effective sensitivity of the observations.

Pure rotational lines of ammonia are also expected in comets but they fall at relatively higher frequencies (submillimeter or far-infrared wavelength region) and are strongly absorbed by the telluric atmosphere. The rotational line of ammonia at 572 GHz was tentatively detected in comets C/2001 Q4 (NEAT) and C/2002 T7 (LINEAR) by the *Odin* satellite (Biver et al. 2007). Future observations from *Herschel* and/or SOFIA will likely improve detections in this wavelength range, though it may be difficult to obtain accurate rotational temperatures.

Several vibrational fundamental bands of NH_3 are accessible from the ground at wavelengths near 3 μm (ν_1, ν_3) and 10 μm (ν_2). The very strong 10 μm band was sought initially using heterodyne and FTIR techniques, but Weaver & Mumma (1984) showed that the near-infrared region was preferred for cometary detections. Rovibrational transitions of ammonia have been observed near 3 μm in comets from ground-based infrared observatories (Bonev et al. 2009; Magee-Sauer et al. 2002, 2006, 2007, 2008; Dello Russo et al. 2007, 2009a, 2009b). Recent progress in high-dispersion echelle spectrometers allows us to sample these rovibrational lines in comets. In contrast with radio observations, the spatial resolution is usually much higher at near-infrared wavelengths and the dilution effect is negligible. However, emission lines of other cometary gases sometimes contaminate those of ammonia, and lines of atmospheric water (mainly) can extinguish some individual lines of NH_3.

Dello Russo et al. (2007, 2009a, 2009b) presented *g*-factors (fluorescence efficiencies) for ammonia emission lines in the near-infrared region, based on a solar fluorescence excitation model. They adopted the line strengths of ammonia measured at room temperature (296 K; Kleiner et al. 1999), assumed that the band strengths are independent of temperature, and estimated the pumping rate for each vibrational band in the solar radiation field (approximated as a blackbody radiation field). Magee-Sauer et al. (2006, 2007, 2008) independently estimated *g*-factors for ammonia in comets based on a similar approach.

In this paper, we present an improved model for fluorescence excitation of NH_3 line-by-line emission in the ν_1 and ν_3 bands. Our new model incorporates fluorescence cascade, for the first time, whereas all previous models were based on fluorescence pumping in a fundamental band only. Our model is based on a more realistic solar spectrum, and it accommodates all significant lines in each band. We present results for five rotational temperatures in the range 20–150 K.

Ammonia in cometary comae is photodissociated into NH_2 by solar UV radiation with a branching ratio of about 95%. The

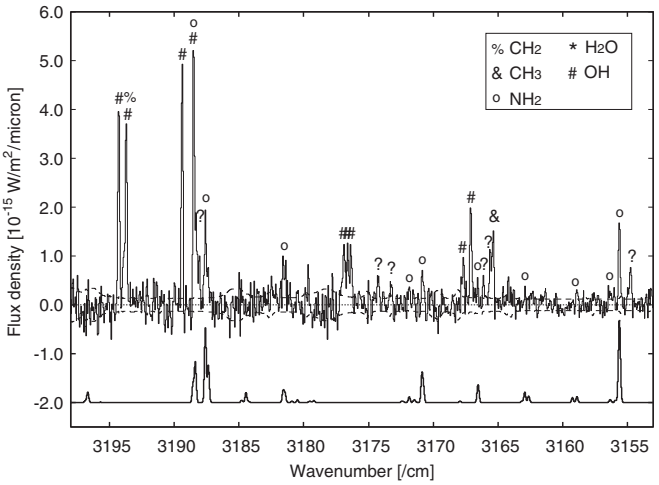

Figure 1. Spectrum of comet C/2004 Q2 Machholz (upper trace) on UT 30.3 2008 January shows spectral lines of NH_2 and other coma species (Kobayashi & Kawakita 2009). The modeled NH_2 spectrum ($T_{rot} = 64$ K, OPR = 3.0) for solar-pumped infrared fluorescence confirms the NH_2 detection (lower trace). The strength of the observed line at 3181.5 cm^{-1} cannot be explained by the NH_2 model and may indicate contamination by unidentified emission lines or the presence of prompt emission from NH_2.

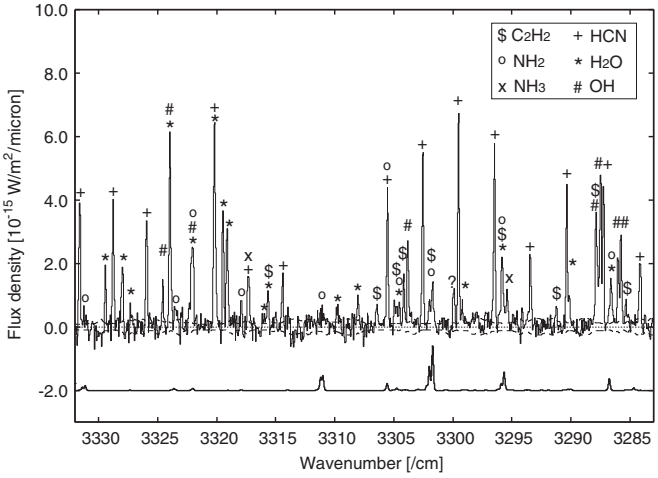

Figure 2. Comparison of the modeled spectrum of NH_2 ($T_{rot} = 64$ K, OPR = 3.0, thick solid line in the lower trace) and the observed spectrum of C/Machholz with error levels (thin solid and dashed lines in the upper spectrum). The emission line of ammonia (marked by "X") at 3295.4 cm^{-1} is contaminated by weak NH_2 lines. The NH_3 line at 3317.3 cm^{-1} is contaminated by the strong HCN line (R1 in the ν_3-band).

amidogen (NH_2) radical can provide an independent means for assessing ammonia in comets, if it is assumed that all NH_2 is produced solely from NH_3 and if the excitation of NH_2 emission is understood. Early analyses of NH and NH_2 suggested that NH_3 was likely the sole parent (Tegler & Wyckoff 1989), but this may not be true for all comets. A comparison of production rates for NH_2 and NH_3 in comets can test this hypothesis, and the prospect of their simultaneous measurement at infrared wavelengths near 3 μm stimulated this research.

The NH_2 radical is long-lived and its strong electronic band system at optical wavelengths has been used to infer the ammonia production rate and abundance ratios for its nuclear spin species (ortho-to-para ratio) in comets (e.g., Kawakita et al. 2001, 2002, 2004, 2006, 2007). In addition to these optical transitions, emission lines associated with N–H stretching vibrations have been recognized in near-infrared spectra of comets (e.g., Mumma et al. 2001; Dello Russo et al. 2006, 2009a, 2009b). While an emission model for the optical band of NH_2 is well developed (Tegler & Wyckoff 1989; Kawakita et al. 2001), no general models for the near-infrared emission lines have been presented so far.

In this article, we present an improved fluorescence excitation model for cometary ammonia in the near-infrared. We apply our model to spectra of comet C/2004 Q2 (Machholz) (hereafter C/Machholz) and derive the production rate of NH_3 in this comet. We also present a near-infrared emission model for NH_2 in comets and apply it to the multiple lines of NH_2 detected in the near-infrared spectra of comet C/Machholz. We compare the production rates of ammonia retrieved independently from measurements of NH_3 and NH_2 in C/Machholz and briefly discuss aspects of prompt emission from NH_2 excited by photolysis of NH_3.

2. SPECTROSCOPIC DATA

The high-dispersion near-infrared spectra of comet C/Machholz used here were acquired with the NIRSPEC spectrometer at the Keck-2 telescope atop Mauna Kea, Hawaii (McLean et al. 1998). C/Machholz was a dynamically new comet from the Oort Cloud, and it became brightest in 2005 January (near perihelion). The near-infrared spectroscopic observations were performed on 2005 January 30.22 UT. The heliocentric and geocentric distances of the comet were 1.208 and 0.480 AU (the heliocentric and geocentric velocities of the comet were +1.83 km s^{-1} and +15.6 km s^{-1}, respectively). A slit of 0.43 by 24 arcsec (corresponding to $\lambda/\Delta\lambda = 25{,}000$) was used.

The observational sequence of "ABBA" was used. C/Machholz was placed at two different positions (A and B) for the observations and (A−B−B+A) was calculated to subtract sky background emission. The nod distance between the A and B positions was 12 arcsec. Detailed information about the observations and data reduction is given elsewhere (Kawakita & Kobayashi 2009; Kobayashi & Kawakita 2009).

Kawakita & Kobayashi (2009) extracted the comet signal within an area of 0.43 × 1.8 arcsec centered on the nucleus, corresponding to dimensions of 150 × 627 km at the comet. Thus, the tangent distance to the nucleus was less than 314 km. The effective rotational temperature of water in this spectral extract was estimated to be 85 ± 5 K, and the water production rate was (2.9 ± 0.1) × 10^{29} molecules s^{-1} (Kawakita & Kobayashi 2009).

Selected spectra are shown in Figures 1–3. Table 1 lists the fluxes measured for individual spectral lines of NH_3 and NH_2 in the comet. The tabulated g-factor for an individual line represents the free space fluorescence efficiency multiplied by the atmospheric transmittance at the Doppler-shifted frequency when observed. Note that we could not find any emission lines of NH_3 that were not contaminated with other molecular emission lines in the observed spectra. We found only two emission lines of NH_3 (at 3317.3 cm^{-1} and 3295.4 cm^{-1}) contaminated with NH_2 and HCN emission lines, respectively (see Table 1). In Figures 1–3, we also compare the observed lines of NH_3 and NH_2 with intensities predicted with models developed for that purpose. The emission line of NH_3 at 3295.4 cm^{-1} is blended with a line of NH_2 whose contribution may be

Table 1
Measurements of Line Flux of NH_3 and NH_2 in C/2004 Q2 (Machholz)

Wavenumber at Rest (cm^{-1})	Flux (10^{-20} W m^{-2})	Line Assignment	Wavenumber at Lab. (cm^{-1})	g-factor[a] (10^{-26} W)	
3295.41	22.8 ± 1.4	NH_3 ν_1 $a^qP(2,1)$	3295.43	2.04	7.43
		NH_3 ν_1 $a^qP(2,0)$	3295.39	5.56	
		NH_2 ν_3 2_{21}–2_{20} (F_1)	3295.52	0.771	1.32
		NH_2 ν_3 2_{21}–2_{20} (F_2)	3295.48	0.452	
		NH_2 ν_3 1_{11}–1_{10} (F_2→F_1)	3295.41	0.0956	
3155.61	31.0 ± 2.0	NH_2 ν_1 2_{02}–3_{13} (F_1)	3155.64	57.1	95.8
		NH_2 ν_1 2_{02}–3_{13} (F_2)	3155.58	36.7	
		NH_2 ν_1 2_{02}–3_{13} (F_1→F_2)	3155.52	2.05	
3187.55	39.6 ± 2.3	NH_2 ν_1 0_{00}–1_{11} (F_1)	3187.60	74.8	112.0
		NH_2 ν_1 0_{00}–1_{11} (F_1→F_2)	3187.37	37.2	
3181.51[b]	20.7 ± 1.8	NH_2 ν_1 4_{13}–4_{22} (F_1)	3181.59	11.9	20.8
		NH_2 ν_1 4_{13}–4_{22} (F_2)	3181.45	8.93	
3170.82	13.0 ± 1.7	NH_2 ν_1 1_{01}–2_{12} (F_1)	3170.88	26.1	38.6
		NH_2 ν_1 1_{01}–2_{12} (F_2)	3170.76	12.5	
3166.56	8.31 ± 1.84	NH_2 ν_1 2_{12}–3_{03} (F_2)	3166.57	7.27	19.9
		NH_2 ν_1 2_{12}–3_{03} (F_1)	3166.51	12.6	
3162.74	8.54 ± 1.84	NH_2 ν_1 3_{13}–3_{22} (F_1)	3162.93	9.75	17.9
		NH_2 ν_1 3_{13}–3_{22} (F_2)	3162.63	6.72	
		NH_2 ν_1 3_{13}–3_{22} (F_1→F_2)	3162.52	0.361	
		NH_2 ν_1 5_{23}–5_{32} (F_2)	3162.93	1.03	
3155.61	31.0 ± 2.0	NH_2 ν_1 2_{02}–3_{13} (F_1)	3155.64	57.1	95.8
		NH_2 ν_1 2_{02}–3_{13} (F_2)	3155.58	36.7	
		NH_2 ν_1 2_{02}–3_{13} (F_1→F_2)	3155.52	2.05	
3317.31	30.2 ± 2.0	NH_3 ν_1 $s^qP(1,0)$	3317.21	2.96	
		HCN ν_3 R1	3317.33	19.9	
...	285 ± 2.2	HCN ν_3 P3+P4+P5[c]	...	263.4	

Notes.
[a] Fluorescence efficiencies include telluric transmittance for conditions of the observations. The heliocentric and geocentric velocities of the comet (+1.83 km s^{-1} and +15.6 km s^{-1}, respectively) were taken into account. The rotational temperatures are assumed to be 85 K for both ammonia and HCN, and 64 K for NH_2. The OPRs of ammonia and NH_2 are assumed equal to their nuclear-spin statistical weight ratios.
[b] This line is eliminated from analysis (see the text).
[c] These HCN lines are used to infer the contamination of the line at 3317.31 cm^{-1} by HCN.

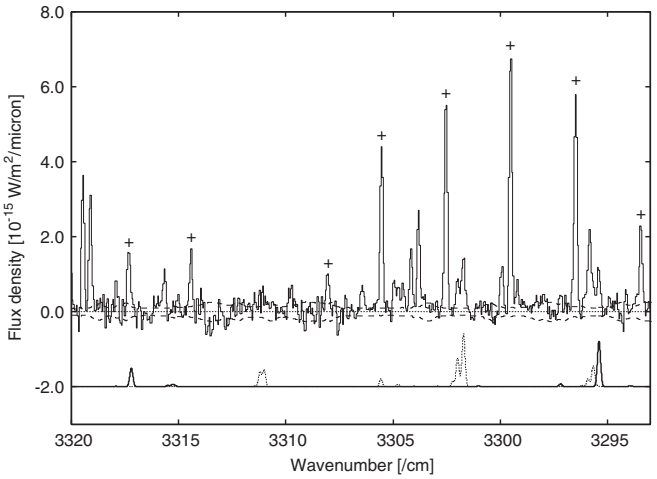

Figure 3. Comparison of the modeled spectrum of NH_3 (T_{rot} = 85 K, OPR = 1.0, thick solid line in the lower spectrum) and the observed spectrum of C/Machholz with error levels (thin solid and dashed lines in the upper spectrum). The modeled spectrum of NH_2 (Figure 2) is shown here as a thick dotted line (lower trace), and the HCN lines are marked by "+" in the figure.

estimated with the new fluorescence excitation model. We defer further discussion of the synthetic and observed intensities to Section 4.

3. EXCITATION MODELS FOR AMMONIA AND NH_2 RADICAL

3.1. Ammonia (NH_3)

In this section, we develop an improved fluorescence model for NH_3 and apply it to observations of C/Machholz described above. Our basic approach is similar to that employed by Dello Russo et al. (2007, 2009a, 2009b) and Magee-Sauer et al. (2006, 2007, 2008), but the details differ significantly as described below.

Kleiner et al. (1999) measured line intensities and positions for three bands of $^{14}NH_3$ (ν_1, ν_3, $2\nu_4$) at room temperature (296 K). Dello Russo et al. (2007, 2009a, 2009b) modeled g-factors for lines of ν_1 using these integrated band strengths and equations for individual transition intensities, Hönl–London factors and Herman–Wallis parameters given by Pine & Dang-Nhu (1993), and Einstein A coefficients for individual rovibrational transitions from the HITRAN database (Rothman et al., 2005). They assumed that the integrated band strengths are independent of temperature and approximated the solar radiation field as a blackbody with a temperature of 5770 K. Dello Russo et al. (2009a) tabulated g-factors for 26 selected lines of ν_1 at one rotational temperature (T_{rot} = 150 K) while Dello Russo et al. (2009b) also tabulated g-factors for two lines of ν_1 at T_{rot} = 40 K. Magee-Sauer et al. (2006, 2007, 2008)

independently estimated g-factors for ammonia in comets using a similar approach. Both groups assumed that rotational populations in the vibrational ground state were characterized by a Boltzmann distribution ($T_{\rm rot}$) and that fluorescence was pumped solely in the fundamental band under consideration, and that re-emission was determined by Einstein A coefficients for downward transitions from the excited rovibrational level.

Here, we do not use the integrated band g-factor at room temperature (based on Kleiner et al. 1999) and we have never assumed that the integrated band g-factor is independent of temperature. The g-factors of individual lines are directly calculated based on Einstein B coefficients using a more realistic solar radiation spectrum with Fraunhofer lines included. Einstein A and B coefficients are calculated from the tabulated line strengths in the HITRAN 2008 database (Rothman et al. 2009) with proper statistical weights according to Šimečková et al. (2006). Note that the Einstein A coefficients tabulated in the HITRAN database are sometimes incorrect (this is the reason why we calculated Einstein A and B coefficients from the tabulated line strengths by ourselves).

Ammonia (NH_3) is a pyramidal shape (symmetric top) molecule that has three identical hydrogen nuclei. The rotational energy of NH_3 depends on two principal quantum numbers (J, K) that correspond to the total angular momentum and its projection along the molecular axis (which is through the nitrogen atom and perpendicular to the plane containing the three hydrogen atoms). Dipole transitions between K-ladders (each K-ladder has energy levels with the same K value, and $J \geqslant K$) are basically forbidden since the dipole selection rules are $\Delta K = 0$ and $\Delta J = 0, \pm 1$. Interaction between rotational and vibrational motions induces a small dipole moment and it gives very slow transitions with $\Delta k = \pm 3$ ($K = |k|$). Therefore, NH_3 in the upper states within each K-ladder (i.e., $J > K$) can decay rapidly ($\sim$10–10^2 s) to the "meta-stable" state ($J = K$) through the $\Delta J = -1$ transitions while the lowest states within each K-ladder (meta-stable states) can only decay via much slower transitions with $\Delta k = \pm 3$ ($\sim 10^9$ s).

Intermolecular collisions also allow transitions in which Δk is a multiple of 3 (including 0) (Oka 1968) and the meta-stable states could be populated via $\Delta k = \pm 3$ collisions. Thus, intermolecular collisions play an important role in determining the population distribution among rotational energy levels of NH_3. As for water, electron collisions are also important (Xie & Mumma 1992). Furthermore, the molecules are classified into two nuclear spin modifications, ortho-ammonia and para-ammonia, with total nuclear spin $I = 3/2$ and $1/2$, respectively. Their spin statistical weights take the familiar values $2I + 1$, respectively 4 (ortho-NH_3) and 2 (para-NH_3). Ortho-ammonia has $K = 3n$ ($n = 0, 1, 2, \ldots$) while para-ammonia has $K = 3n+1$ or $K = 3n+2$ ($n = 0, 1, 2, \ldots$) in their vibrational ground state. Transitions among ortho- and para-states are forbidden, hindering the inter-conversion of ortho- and para-ammonia. The symmetry of the wave function (s, a) upon inversion through the plane containing the three hydrogen atoms introduces a final quantum number.

In the inner coma, intermolecular collisions can be so frequent that ammonia molecules are promoted into higher energy levels ($J > K$) within each K-ladder. Here, we assume that the population distribution in the ground vibrational state of ammonia molecules is maintained in a Boltzmann rotational distribution (characterized by a temperature, $T_{\rm rot}$) by frequent intermolecular collisions (mainly with water molecules). The NH_3 molecules in the vibrational ground state could be excited to the vibrational excited states by the solar radiation field. Thus, we can observe photons emitted by the downward transitions from the vibrational excited states to the vibrational ground state.

This simple model is successful in the case of H_2O, CO, HCN, CH_4, and so on in comets. However, when a comet is not so productive (namely, gas density in the coma is lower and less frequent collisions occur), the fluorescence excitation model of NH_3 must include relaxation in the ground vibrational state via radiative rotational transitions ($\Delta J = \pm 1$) at far-infrared wavelengths. For the production rate retrieved on January 30, collision rates of ammonia with water within about 500 km from the nucleus are estimated to be higher than the typical Einstein A coefficients for $\Delta J = \pm 1$ within each K-ladder (0.1–0.01 s^{-1}). Thus, our assumption of a Boltzmann distribution in the vibrational ground state is acceptable in this case.

We consider not only direct excitation of ν_1 and ν_3 by the solar radiation field, but also cascades from upper vibrational states combining two or more vibrations (e.g., $\nu_1 + \nu_2$). The vibrational hot bands (e.g., $(\nu_1 + \nu_2) - \nu_1$) and related excitations from the ground state to the upper vibrational combined states (e.g., $(\nu_1 + \nu_2)$) are also included in the model. Such cascades were not considered in previous studies. Eventually, we considered the vibrational states of ν_1, ν_2, $2\nu_2$, $3\nu_2$, ν_3, ν_4, $(\nu_1 + \nu_2)$, $(\nu_1 + \nu_4)$, $(\nu_2 + \nu_3)$, and $(\nu_3 + \nu_4)$. Their related transitions (cold bands for each state and hot bands of $(\nu_1 + \nu_2) - \nu_1$, $(\nu_1 + \nu_4) - \nu_1$, $(\nu_2 + \nu_3) - \nu_3$ and $(\nu_3 + \nu_4) - \nu_3$) are involved in the model. On the other hand, we neglect vibrational excitation and quenching by collisions with neutral molecules and with electrons. As briefly described above, we calculated Einstein A and B coefficients for the transitions within these bands based on the HITRAN database. These coefficients were computed from the line strengths tabulated there, following Šimečková et al. (2006) for transitions within cold bands. For the hot bands, we assumed that vibrational modes are separable (the Born approximation). In this case, Einstein A coefficients within a hot band (e.g., the ν_2 hot band, $(\nu_1 + \nu_2) - \nu_1$) are the same as those for the corresponding fundamental band (e.g., ν_2 fundamental band). Einstein B coefficients for stimulated emission are obtained from corresponding Einstein A coefficients.

The pumping rate is estimated from the Einstein B coefficients for spontaneous absorption (obtained from tabulated line strengths for fundamental and combination bands) and the solar radiation field at 1 AU (Hase et al. 2010; Kurucz 1994, 2005), and is scaled to another heliocentric distance by using a scaling law of r^{-2} (r denotes a heliocentric distance in AU). Figure 4 shows the example of solar radiation density at 1 AU.

For the ith energy level in the excited vibrational state (such as the ν_1 state), the condition of detailed balance (i.e., a balance between outgoing and incoming rates for the level) becomes

$$n_i \sum_j (A_{ij} + B_{ij}\rho_\odot(\nu_{ij})) = \sum_j (n_j B_{ji}\rho_\odot(\nu_{ij})) + \sum_k n_k (A_{ki} + B_{ki}\rho_\odot(\nu_{ki})), \quad (1)$$

where n_i is the population in the ith energy level and $\rho_\odot$ is the energy density of the solar radiation at a given heliocentric distance. The ν_{ij} is the wavenumber corresponding to the transition between the ith and the jth energy levels (the jth energy levels are in the ground state) while A_{ij} and B_{ij} are Einstein A

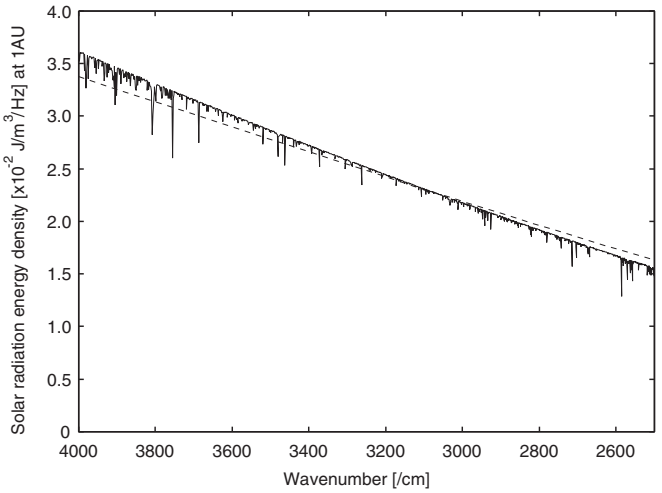

Figure 4. Example of the solar radiation energy density at 1 AU from the Sun (solid line) and the blackbody spectrum at 5770 K as comparison (dashed line). Fraunhofer absorption lines can affect g-factors of molecular emission lines pumped in the near-infrared. After Hase et al. (2010).

and B coefficients between the ith and the jth energy levels. The kth energy levels are in the more excited vibrational state, e.g., (ν_1+ν_2) state for the ν_1 state. Note that the effective value of $\rho_\odot$ depends on the relative velocity of the comet to the Sun since there are many absorption lines in the solar spectrum and they are much wider than the Doppler profile of the cometary gas. The g-factor (g_{ij} (photons s^{-1})) for a transition is based on the fractional populations (n_j) in the lower energy levels (which are calculated from the Boltzmann distribution for the adopted rotational temperature; see the discussion above), the solar pumping rates ($B_{ji}\rho_\odot(\nu_{ji})$), and the branching ratio for spontaneous emission into the transition in question at ν_{ij}. The population in each level can be determined by solving the linear equations (Equation (1)). Thus, the g-factor is given by

$$g_{ij} = n_i A_{ij} = \frac{\sum_j (n_j B_{ji} \rho_\odot(\nu_{ij})) + \sum_k n_k (A_{ki} + B_{ki}\rho_\odot(\nu_{ki}))}{\sum_j (A_{ij} + B_{ij}\rho_\odot(\nu_{ij}))} A_{ij}.$$

Because ortho–para transitions are strictly forbidden, the populations may be regarded as representing either ortho- or para-NH_3. We assume that the level population for a given spin species is described by a temperature, but the formalism admits any abundance in the ortho and para species. The abundance ratio of ortho- and para-ammonia is 1.0 in statistical equilibrium. However, the ratio is probably greater than unity (∼1.1) as determined in some comets based on NH_2 observations (Kawakita et al. 2001, 2002, 2004, 2006, 2007). Such nonequilibrated ortho-to-para abundance ratio (OPR) of ammonia could be interpreted as the result of ammonia formation on cold grain surface in the pre-solar molecular cloud or in the solar nebula. For the present purpose of model development, we assume that the OPR of ammonia is unity, i.e., in statistical equilibrium.

Figure 5 illustrates the vibrational bands considered here (in the case of the observations of C/Machholz). If we consider fundamental bands only, the band g-factors are the same as the corresponding pumping rates (e.g., 2.17 × 10^{-5} s^{-1} for the ν_1 fundamental band). However, the band g-factor of ν_1 increases by ∼15% if we include cascades from higher excited states. Furthermore, the band g-factor of ν_3 increases by a factor of ∼2 if the cascades are included in the model (Table 2 lists g-factors for selected lines).

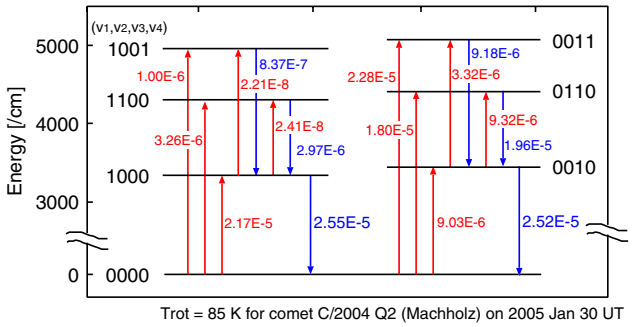

Figure 5. New model for solar-pumped fluorescence of the ν_1 and ν_3 bands of ammonia includes pumping by fundamental and combination bands followed by either resonant or non-resonant decay, as represented in the diagram. We evaluated the solar pumping rates (upward arrows (red) labeled by pumping rates in (s^{-1})) for conditions experienced by C/Machholz on UT 30.22 2005 January (r = 1.209 AU, $\dot{r}$ = +1.83 km s^{-1}). The rotational temperature in the ground vibrational state and the OPR are assumed to be 85 K and unity, respectively. Downward arrows (blue) represent radiative decay and are labeled with the g-factor (in photons s^{-1}) for that transition summed over both direct and cascade contributions. Downward transition rates from combination bands to the ground state are omitted for the readability (those rates are 3.15 × 10^{-7}, 1.85 × 10^{-7}, 7.67 × 10^{-6}, and 1.69 × 10^{-5} for ν_1+ν_2, ν_1+ν_4, ν_2+ν_3, and ν_3+ν_4 bands, respectively). Cascade increases the band g-factor for the ν_1 band by 17.5% over direct excitation by fundamental band pumping alone. For the ν_3 band, cascade increases the band g-factor by 179% over that from fundamental band pumping alone. The cascade model thus increases the band g-factors by factors of 1.17 (ν_1) and 2.79 (ν_3), respectively, compared to the values for models with fundamental band pumping alone.

(A color version of this figure is available in the online journal.)

Table 3 also lists some selected lines with g-factors published elsewhere (Dello Russo et al. 2009a, 2009b). The difference between our g-factors and those published in previous studies is modest for the ν_1 fundamental band (Dello Russo et al. did not consider the cascades from higher excited states). It is not easy to specify the contributions of competing effects to the final difference in g-factors between the two models. We used the solar spectrum containing Fraunhofer lines that introduce reduced pump efficiency at some Doppler shifts, while previous models used a blackbody spectrum. Note that g-factors based on the actual solar spectrum could be larger than those based on the blackbody spectrum at 5770 K in some cases since the continuum level of the solar spectrum does not fit the blackbody spectrum exactly (Figure 4). Also, Einstein A coefficients used by Dello Russo et al. might differ from ours (if they used the Einstein A coefficients listed in the HITRAN database). We found that the statistical weights of some lines are incorrect in the HITRAN database (at least, until 2009) and the Einstein A coefficients computed from the line strengths with correct statistical weights are different from those tabulated in the database as we noted above.

Table 4 lists the g-factors for individual lines of ammonia ν_1 and ν_3 at 1 AU from the Sun (the comet's heliocentric velocity is assumed to be 0 km s^{-1}) for various rotational temperatures ($T_{\rm rot}$ = 20, 70, 100, 120, and 150 K) that span the range of $T_{\rm rot}$ seen in most comets.

3.2. NH_2 Radical

Photolysis of ammonia by solar UV radiation in the coma produces NH_2 with 95% efficiency. Because NH_2 has a long lifetime against photodissociation (see below), its strong rovibronic band at optical wavelengths is often seen in cometary comae (Feldman et al. 2004 and references therein).

The principal mechanism for excitation of the NH_2 optical band is by solar fluorescence, and excitation models for

Table 2
Comparison Between g-factors of NH_3 With and Without Cascades for Selected Lines

Wavenumber (cm^{-1})	Line Assignment	g-factor (photons s^{-1}) (for Observations of C/Machholz)	
		Without Cascades	With Cascades
3376.27	ν_1 sqR(1,0)	9.00×10^{-7}	1.05×10^{-6}
3376.33	ν_1 sqR(1,1)	3.36×10^{-7}	3.59×10^{-7}
3336.39	ν_1 sqQ(3,3)	1.02×10^{-6}	1.19×10^{-6}
3334.60	ν_1 aqQ(3,3)	9.97×10^{-7}	1.18×10^{-6}
3295.39	ν_1 aqP(2,0)	1.02×10^{-6}	1.19×10^{-6}
3295.43	ν_1 aqP(2,1)	3.71×10^{-7}	3.99×10^{-7}
3478.20	ν_3 srR(1,0)	2.26×10^{-7}	5.01×10^{-7}
3470.74	ν_3 srR(1,1)	1.90×10^{-7}	4.05×10^{-7}
3461.95	ν_3 spQ(3,3)	3.23×10^{-8}	1.10×10^{-7}
3461.48	ν_3 apQ(3,3)	3.19×10^{-8}	9.97×10^{-8}
3398.99	ν_3 arP(2,0)	2.59×10^{-7}	3.90×10^{-7}

Table 3
Comparison of Our g-factors of NH_3 and Those of Dello Russo et al. (2009a, 2009b)

Wavenumber (cm^{-1})	Line Assignment	g-factor (photons s^{-1})		
		Dello Russo et al. (2009a) for $T_{rot} = 150$ K at $r =$ 0.554 AU[a]	This work for $T_{rot} = 150$ K at $r = 0.554$ AU (but for BB radiation field at 5770 K)[b]	This work for $T_{rot} = 150$ K at $r = 0.554$ AU
3336.39	ν_1 sqQ(3,3)	4.46×10^{-6}	4.69×10^{-6}	4.75×10^{-6}
3335.98	ν_1 sqQ(4,4)	1.87×10^{-6}	1.85×10^{-6}	1.86×10^{-6}
3335.64	ν_1 sqQ(4,3)	2.02×10^{-6}	2.10×10^{-6}	2.16×10^{-6}
3334.60	ν_1 aqQ(3,3)	4.40×10^{-6}	4.62×10^{-6}	4.74×10^{-6}
3334.39	ν_1 aqQ(3,2)	9.48×10^{-7}	9.30×10^{-7}	9.42×10^{-7}
3334.28	ν_1 aqQ(3,1)	2.31×10^{-7}	2.23×10^{-7}	2.25×10^{-7}
		Dello Russo et al. (2009b) for $T_{rot} = 40$ K at $r = 1.354$ AU[a]	This work for $T_{rot} = 40$ K at $r = 1.354$ AU (but for BB radiation field at 5770 K)[b]	This work for $T_{rot} = 40$ K at $r = 1.354$ AU
3376.3	ν_1 sqR(1,0) + sqR(1,1)	1.79×10^{-6}	1.86×10^{-6}	1.92×10^{-6}
3295.4	ν_1 aqP(2,0) + aqP(2,1)	2.53×10^{-6}	2.53×10^{-6}	2.60×10^{-6}

Notes.
[a] The g-factors are at r [AU], scaled by the r^2 law. These values are based on the fluorescence excitation model without cascades and the solar spectrum is approximated by a blackbody spectrum at 5770 K (N. Dello Russo 2010, private communication).
[b] These values are based on our fluorescence excitation model with cascades, but using blackbody spectrum as the solar spectrum.

Table 4
The g-factors for Lines of NH_3 ν_1 and ν_3 at 1 AU ($\dot{r} = 0$ km s^{-1})

Wavenumber	g-factor (photons s^{-1})					Assignment
(cm^{-1})	$T_{rot} = 20$ K	$T_{rot} = 70$ K	$T_{rot} = 100$ K	$T_{rot} = 120$ K	$T_{rot} = 150$ K	
3415.11	1.23E-08	2.97E-07	3.59E-07	3.70E-07	3.64E-07	ν_1 sqR(3,3)
3414.83	1.55E-08	2.19E-07	2.64E-07	2.72E-07	2.68E-07	ν_1 sqR(3,2)
3414.69	1.52E-08	2.56E-07	3.14E-07	3.24E-07	3.20E-07	ν_1 sqR(3,1)
3414.64	2.26E-08	5.78E-07	7.17E-07	7.43E-07	7.36E-07	ν_1 sqR(3,0)
3413.32	1.15E-08	2.87E-07	3.49E-07	3.60E-07	3.55E-07	ν_1 aqR(3,3)
3413.09	1.58E-08	2.16E-07	2.61E-07	2.69E-07	2.66E-07	ν_1 aqR(3,2)
3412.96	1.48E-08	2.46E-07	3.02E-07	3.12E-07	3.09E-07	ν_1 aqR(3,1)
3395.76	1.71E-07	3.36E-07	3.06E-07	2.82E-07	2.48E-07	ν_1 sqR(2,2)
3395.60	2.80E-07	5.42E-07	4.86E-07	4.44E-07	3.88E-07	ν_1 sqR(2,1)
3393.99	1.65E-07	3.33E-07	3.04E-07	2.81E-07	2.47E-07	ν_1 aqR(2,2)

(This table is available in its entirety in a machine-readable form in the online journal. A portion is shown here for guidance regarding its form and content.)

line-by-line intensities do exist (Kawakita et al. 2001). In recent years, high-resolution infrared spectra of comets have revealed emission lines of NH_2 rovibrational bands (ν_1 and ν_3) near 3 μm, but excitation models for them are lacking. We now address these models.

Near-infrared high dispersion spectra often sample a very narrow region close to the nucleus, as in the case of C/Machholz. The NH_2 radicals sampled within the small aperture could experience frequent intermolecular collisions (mainly with water molecules) and with electrons, and NH_2 radicals may not be able to achieve fluorescence equilibrium in the inner coma. For this reason, we developed a fluorescence model for NH_2, in which the ground vibrational state is assumed to be at thermal equilibrium.

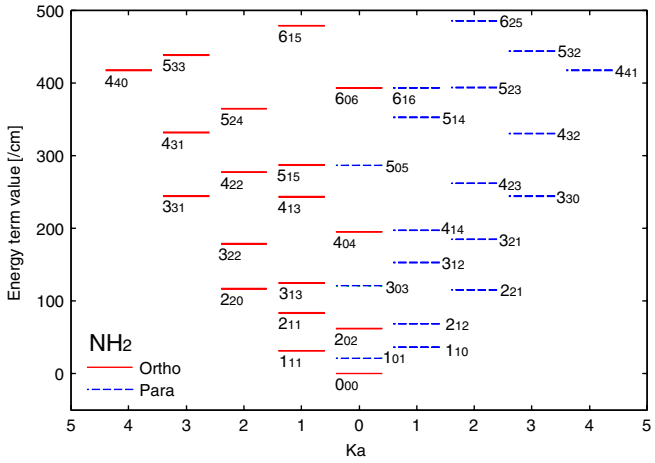

Figure 6. Energy level diagram of NH_2 in the vibrational ground state. Different nuclear spin levels are shown in different colors (solid red lines for ortho-NH_2 and dashed blue lines for para-NH_2).

(A color version of this figure is available in the online journal.)

NH_2 is an asymmetric molecule and its energy structure is more complicated than a symmetric top molecule like ammonia (Herzberg 1966). Since NH_2 has an unpaired electron, each rotational energy level is split into two sub-levels ("fine structure"). The line splitting caused by nuclear spin of the nitrogen atom ("hyperfine structure") cannot be resolved by the optical and near-infrared spectroscopic instruments currently available (typical spectral resolving power, $\lambda/\Delta\lambda < 10^6$). The energy levels of NH_2 are classified into ortho ($I = 1$) and para ($I = 0$) states according to the relative orientations of the individual proton spins. Figure 6 shows the energy level diagram of NH_2 molecule in the vibrational ground state, $\tilde{X}(0,0,0)$.

We include the following transitions in our model: (1) rovibrational transitions between $\tilde{X}(1,0,0)$–$\tilde{X}(0,0,0)$ and $\tilde{X}(0,0,1)$–$\tilde{X}(0,0,0)$; and (2) rovibronic transitions between $\tilde{A}(1,v_2',0)$–$\tilde{X}(0,0,0)$ and $\tilde{A}(1,v_2',0)$–$\tilde{X}(1,0,0)$ where $v_2' = 5$–8. The ground state $\tilde{X}(0,0,0)$ is assumed to follow the Boltzmann distribution (which is considered to be maintained by frequent intermolecular and/or electron collisions). Rotational levels with $N' \leqslant 5$ are included in our model. We found that the rovibronic transitions between $\tilde{A}(1,v_2',0)$–$\tilde{X}(0,0,0)$ and $\tilde{A}(1,v_2',0)$–$\tilde{X}(1,0,0)$ are more important for populating the $\tilde{X}(1,0,0)$ state than in direct pumping from $\tilde{X}(0,0,0)$ to $\tilde{X}(1,0,0)$. The transition probabilities of the $\tilde{A}(1,v_2',0)$–$\tilde{X}(0,0,0)$ bands are comparable to those of the $\tilde{A}(0,v_2',0)$–$\tilde{X}(0,0,0)$ bands that are usually observed in optical spectra of comets. The importance of the transitions between $\tilde{A}(1,v_2',0)$ and $\tilde{X}(0,0,0)$ or $\tilde{X}(1,0,0)$ originates in the Fermi resonance between the states of $\tilde{A}(1,v_2',0)$ and $\tilde{A}(0,v_2'+4,0)$ (Dressler & Ramsay 1959, Ross et al. 1988). Wavenumbers of transitions in the 3 μm region (both ν_1- and ν_3-bands) are taken from McKellar et al. (1990) while wavenumbers of the transitions between $\tilde{A}(1,v_2',0)$ and $\tilde{X}(0,0,0)$ or $\tilde{X}(1,0,0)$ are taken from Dressler & Ramsay (1959) and Ross et al. (1988). Einstein A coefficients are calculated on the basis of the molecular constants (Müller et al. 1999; Burkholder et al. 1988; McKellar et al. 1990) and ab initio calculations of transition moments for vibronic transitions by Jensen et al. (2003).

Table 5 lists the g-factors of NH_2 at 1 AU from the Sun (the relative velocity to the Sun is assumed to be zero) for various rotational temperatures. The OPR of NH_2 is assumed to be 3.0 in both models. Note that the OPRs determined in some comets were slightly larger than 3.0 (Kawakita et al. 2001, 2002, 2004, 2006, 2007) and probably approach ~3.3 for several comets. These relatively higher OPRs in NH_2 than the nuclear spin statistical weight ratio (3.0) were considered to be the result that the cometary ammonia has OPR higher than unity and NH_2 radicals formed from ammonia by photodissociation in coma. Assuming ammonia as the sole parent of NH_2, the OPRs of ammonia were estimated from the OPRs of NH_2 as ~1.1 in the several comets as noted in the previous section.

To date, there are few reports of direct measurement of ammonia in comets, and none that report a value for OPR. Once OPRs are measured routinely, comparison of OPRs for NH_3 and NH_2 can test the presence of a second parent of NH_2. Such tests could be compared with direct measurements of production rates for NH_2 and NH_3 that provide an independent measure of the parentage of NH_2.

4. RESULTS AND DISCUSSION

We next compare the observed and synthetic emission spectra of ammonia and NH_2 in comet C/Machholz. Figures 1–3 show that the modeled spectra of ammonia and NH_2 can reproduce some of the emission lines in the observed spectra.

4.1. Rotational Temperatures of Ammonia and NH_2

As already mentioned toward the end of Section 2, only two NH_3 emission lines (contaminated with NH_2 and HCN, respectively) were detected in the spectra of C/Machholz. Due to the small number of measured lines and the contaminations (especially due to the large contribution of HCN (R1) to the blend at 3317.3 cm^{-1}), it is difficult to determine the T_{rot} (and OPR) based on the measurements of ammonia. Therefore, we modeled the ammonia spectrum by adopting $T_{rot} = 85$ K, the value measured for water on the same night (Kawakita & Kobayashi 2009). The OPR of ammonia is assumed to be unity. The F/g chart (F and g denote the measured line flux and the g-factor of each line, respectively) versus upper energy levels (E') for the ammonia emission lines (Figure 7) tells us that the assumed T_{rot} is consistent with the observations. The line fluxes shown in Figure 7 were obtained from the measured fluxes (Table 1) by removing the contributions of blended NH_2 and HCN lines using correction factors obtained from their modeled spectra. For example, the contribution of HCN (R1) at 3317.3 cm^{-1} was estimated from measured unblended emission lines of HCN (P3, P4, P5) by scaling with a ratio of g-factors (see Table 1). The relative contribution of HCN for the emission line at 3317.3 cm^{-1} is ~70% while that of NH_2 for the emission lines at 3295.4 cm^{-1} is ~2% only.

In contrast with ammonia, we measured multiple NH_2 emission lines that lacked significant contaminations (Table 1), allowing us to determine T_{rot} for NH_2. We found $T_{rot} = 64(+18/-11)$ K by the χ^2-fitting technique. (The best reduced-χ^2 (0.76) was achieved by excluding the emission line of NH_2 at 3181.5 cm^{-1} (4_{13}–4_{22} in the ν_1-band). If we include this line, the best reduced-χ^2 was 4.41, and this fact may indicate the contamination by unidentified emission lines or may indicate the presence of prompt emission lines of NH_2.) The obtained T_{rot} of NH_2 is consistent with the T_{rot} of H_2O (85 ± 5 K) determined from water spectra taken at the same time by Kawakita & Kobayashi (2009). The OPR of NH_2 could not be determined precisely due to relatively large errors, but is consistent with OPR = 3.0 (i.e., a nuclear-spin ratio consistent with statistical equilibrium).

Table 5
The g-factors of NH_2 at 1 AU ($\dot{r} = 0\,km\,s^{-1}$)

Wavenumber	g-factor (photons s^{-1})					(v_1',v_2',v_3')	$J'(K_a'\ K_c')$
(cm^{-1})	$T_{rot} = 20$ K	$T_{rot} = 70$ K	$T_{rot} = 100$ K	$T_{rot} = 120$ K	$T_{rot} = 150$ K	– (v_1",v_2",v_3")	– $J'(K_a"K_c")$
3467	7.40E-15	2.24E-12	5.44E-12	7.34E-12	9.37E-12	(0,0,1)–(0,0,0)	3(31)–2(12)
3466.85	1.03E-13	3.14E-11	7.61E-11	1.03E-10	1.31E-10	(0,0,1)–(0,0,0)	3(31)–2(12)
3466.25	1.65E-13	4.78E-11	1.15E-10	1.55E-10	1.97E-10	(0,0,1)–(0,0,0)	3(31)–2(12)
3452.99	1.41E-13	1.00E-11	2.43E-11	3.28E-11	4.18E-11	(0,0,1)–(0,0,0)	3(30)–2(11)
3452.78	1.97E-12	1.40E-10	3.40E-10	4.58E-10	5.85E-10	(0,0,1)–(0,0,0)	3(30)–2(11)
3452.25	3.14E-12	2.14E-10	5.13E-10	6.90E-10	8.78E-10	(0,0,1)–(0,0,0)	3(30)–2(11)
3419.77	1.40E-11	2.37E-10	3.11E-10	3.33E-10	3.41E-10	(0,0,1)–(0,0,0)	3(21)–2(02)
3419.71	1.96E-10	3.31E-09	4.35E-09	4.66E-09	4.77E-09	(0,0,1)–(0,0,0)	3(21)–2(02)
3419.39	3.09E-10	5.17E-09	6.74E-09	7.18E-09	7.32E-09	(0,0,1)–(0,0,0)	3(21)–2(02)
3396.46	4.20E-09	4.09E-09	3.49E-09	3.19E-09	2.84E-09	(1,0,0)–(0,0,0)	3(31)–2(02)

(This table is available in its entirety in a machine-readable form in the online journal. A portion is shown here for guidance regarding its form and content.)

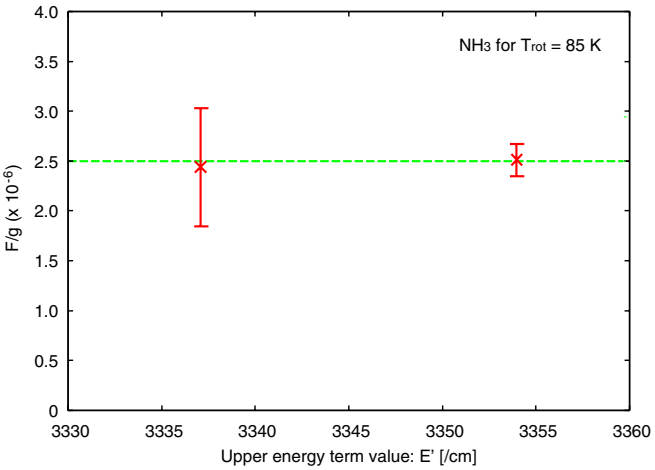

Figure 7. F/g chart vs. upper energy term values for NH_3. Line fluxes shown here were obtained by removing the intensity of blended lines (see the text). We calculated g-factors by adopting the rotational temperature measured for H_2O (85 K) on the same night (Kawakita & Kobayashi 2009). The observed spectra are consistent with the rotational temperature of 85 K. The dashed line is the weighted average of the F/g values.

(A color version of this figure is available in the online journal.)

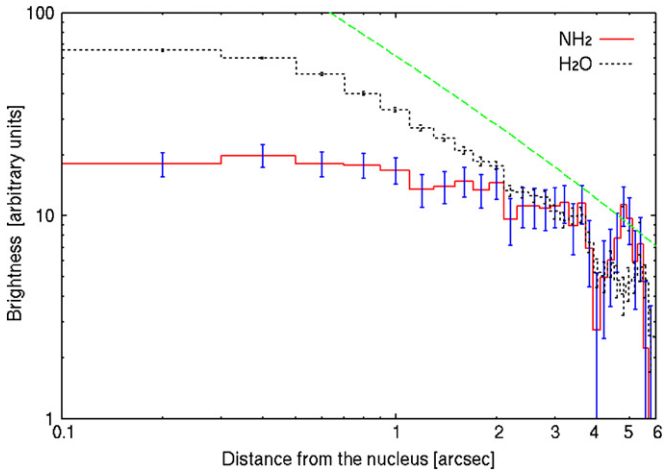

Figure 8. Spatial profiles of NH_2 and H_2O measured simultaneously in echelle spectra of C/Machholz. The spatial distributions of NH_2 (at $\sim$3155.6 cm^{-1}) and H_2O (at 3453.2 and 3450.3 cm^{-1}) are extracted from the echelle spectra by binning intensities measured at symmetric positions about the nucleus. The dashed line (green) corresponds to the ρ^{-1} spatial profile with the correction for the image processing of (A−B−B+A) that introduces over-subtraction of comet signal. Error bars are 1σ levels. At the comet, 1 arcsec subtends a tangent distance of 349 km, and the scale length of ammonia (7000 km) thus represents a tangential distance of 20 arcsec (see Section 4.3).

(A color version of this figure is available in the online journal.)

4.2. NH_3/H_2O Ratio Determined from Ammonia Emission

Once we determine or assume the T_{rot} (and OPR) for ammonia, a production rate of ammonia and a mixing ratio of ammonia with respect to water can be derived by adopting an appropriate model for the spatial distribution of the molecules in the coma. The isotropic expanding coma model (with a constant expansion velocity) is frequently used for the parent molecules (DiSanti & Mumma 2008). The methodology accounts for axisymmetric outflow by taking the mean of spherical production rates obtained at symmetric positions about the nucleus-centered position. The expansion velocity of gas is assumed to be $0.8 \times r^{-0.5}$ km s^{-1} (r denotes a heliocentric distance in AU), and we used the photodissociation rate listed in Huebner et al. (1992) with a scaling law of r^{-2}. Note that the gas production rate mainly depends on the expansion velocity but not significantly on the lifetime (here determined by photodissociation) when we sample parent molecules within the very inner coma (Kobayashi et al. 2007). The "Q-curve" correction (correcting for slit losses; DiSanti & Mumma 2008) was applied for ammonia by assuming the same growth factor as measured for H_2O (these molecules were sampled at the same time). Thus, the resultant production rate of ammonia is $Q(NH_3) = (1.4 \pm 0.1) \times 10^{27}$ molecules s^{-1}, which corresponds to the mixing ratio of $NH_3/H_2O = 0.46\% \pm 0.03\%$ in C/Machholz. Note that the uncertainties in these results represent the stochastic error only. The systematic error (e.g., caused by the coma model used in this study) for NH_3 must be larger than the stochastic error given above.

4.3. Determining the Production Rate of NH_2

Figure 8 shows the spatial profiles of NH_2 and H_2O along the slit. Both species were observed simultaneously at night (Kobayashi & Kawakita 2009). Within 3 arcsec of the nucleus, the spatial profile of NH_2 is flatter than that of H_2O (which follows the expected ρ^{-1} profile of a parent volatile). This behavior of NH_2 is expected for fluorescence from a daughter molecule, and it directly confirms that the observed emission is not prompt emission produced as a consequence of dissociative excitation of the parent (see Section 4.4).

Because NH_2 is very long-lived in the solar radiation field, its spatial profile about the nucleus should vary as ρ^{-1} for nucleocentric distances (ρ) greater than twice the scale length of its production but yet smaller than its destruction scale length, and the fraction of the entire NH_2 in the coma that is sampled by the observations can be determined from its intensity profile in that region. However, if NH_3 is the sole parent of NH_2, these conditions are not satisfied by the present observations. Assuming the lifetime of ammonia is about 7000 s for photodissociation with an outflow velocity of $\sim$0.7 km s^{-1} at 1.2 AU for the observations discussed here, the scale length is about 5000 km. This is much larger than the scale of the sampled region, and it is the reason why the observed NH_2 profile did not follow the ρ^{-1} profile in Figure 8.

Here we apply a random-walk model for NH_2 coma that is based on the Monte Carlo simulation technique (Kawakita & Watanabe 1998). This is more realistic than the Haser model usually used for NH_2 in optical observations because it includes the collisions between molecules explicitly and also includes the excess energy and the random orientation of ejection velocity at photolysis (details are described in Kawakita & Watanabe 1998). The photodissociation lifetimes of parent and NH_2 molecules are specified explicitly in the model. The bulk expansion velocity and kinetic temperature of the surrounding coma are assumed to be $0.8 \times r^{-0.5}$ (km s^{-1}) and 85 K, respectively. The photodissociation rates are taken from Huebner et al. (1992). We can also begin by assuming that NH_3 is the sole parent of NH_2, and then apply the random-walk model for the conditions of C/Machholz, when observed. Photodissociation rates of NH_3 and NH_2 at 1 AU are 1.8×10^{-4} s^{-1} and 2.15×10^{-6} s^{-1}, respectively (Huebner et al. 1992), subject to the r^{-2} heliocentric scaling law. The ejection velocity of NH_2 at photodissociation is assumed to be 0.8 km s^{-1} (Krasnopolsky & Tkachuk 1991).

Thus, the gas production rate of NH_2 ($Q(NH_2)$) is derived to be 2.3×10^{27} (molecules s^{-1}). The synthesized spatial profile is shown in Figure 9. If we use a different estimate of the photodissociation rate of ammonia (4.8×10^{-4} s^{-1} at 1 AU; Jackson 1976a, b), we obtain $Q(NH_2) = 0.9 \times 10^{27}$ molecules s^{-1}. As shown in Figure 9, the spatial profiles for those two parameters are not distinguishable over the small distances sampled by our observations of C/Machholz.

Furthermore, we obtain $Q(NH_2) = 1.3 \times 10^{27}$ molecules s^{-1} from $Q(NH_3)$ obtained by direct measurement of ammonia emission (adopting 0.95 as the yield of NH_2 from photolysis of NH_3). This value falls between the cases shown above (2.3×10^{27} and 0.9×10^{27}) and thus we consider ammonia to be a major source of NH_2. We cannot rule out the possibility of additional sources for NH_2. We need a spatial profile of NH_2 in the coma until 10,000 km or further from the nucleus, observed by a longer slit, to investigate photodissociation lifetime for a parent of NH_2 and to derive $Q(NH_2)$ accurately.

Errors in g-factors of NH_2 may also have to be considered. Clearly, it is better to include weaker transitions between $\tilde{A}(1,v_2',0)$ and $\tilde{X}(0,0,0)$ or $\tilde{X}(1,0,0)$, i.e. $v_2' \neq 5$–8. Transitions between $\tilde{X}(1,v_2',0)$ and $\tilde{X}(0,0,0)$ or $\tilde{X}(1,0,0)$ may also contribute to the g-factors of NH_2. However, we do not have precise laboratory measurements and transition moments for those weaker transitions, so we include in our model only the most prominent bands in the optical region. Additional weaker transitions would increase the population in the $\tilde{X}(1,0,0)$ state slightly and therefore increase g-factors (i.e., $Q(NH_2)$ will slightly decrease).

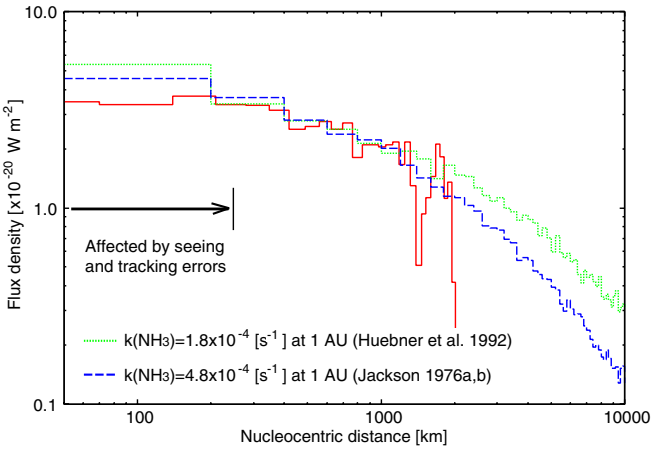

Figure 9. Comparison of observed (red/solid) and modeled (blue/dashed, green/dotted) spatial profiles of NH_2. The synthetic profiles are based on a random-walk model for NH_2 (Kawakita & Watanabe 1998) and the g-factors calculated in this article are used to reproduce the observed spatial profile of NH_2. The increasing over-subtraction of comet signal at nucleocentric distance > 682 km (2″) by the (A−B−B+A) calculation was included in both modeled profiles.

(A color version of this figure is available in the online journal.)

Thus, the NH_3 production rates determined from the ammonia emission and from the NH_2 lines are consistent within errors. Ammonia can produce a sufficient amount of NH_2 radicals in the coma of C/Machholz (i.e., we can consider (but not conclude) that ammonia is the sole parent of NH_2). The mixing ratio of ammonia obtained from detected lines of NH_2 (ν_1 band) is 0.31%–0.79%, assuming 0.95 as the yield of NH_2 from photolysis of NH_3.

4.4. Prompt Emission Lines of NH_2

We also considered the possible presence of occasional prompt emission lines of NH_2 in our spectra. Just after its formation by photodissociation of NH_3 in the coma, the NH_2 radical could be vibrationally and/or rotationally excited as in the case of OH* from H_2O (Mumma et al. 2001; Bonev et al. 2004, 2006; Bonev & Mumma 2006; Dello Russo et al. 2006; Magee-Sauer et al. 2007). An NH_2 radical excited in this way will also emit promptly, with a volume emission rate that is proportional to the local number density of NH_3 in the coma. The spatial profile of NH_2 prompt emission is then proportional to the NH_3 column density, and the prompt emission can be used as a proxy for the parent molecule. Photolysis of H_2O produces OH in highly excited rotational states (in $v' = 1$ and $v' = 2$) and subsequent prompt emission from these levels is easily distinguished from fluorescence pumping of thermalized OH in the coma. We do not know whether prompt emission from highly excited rovibrational states of NH_2 (ν_1 band) is present in C/Machholz, but the spatial profile seen in Figure 8 is not consistent with that of a parent volatile released from the nucleus. If prompt emission is responsible for most NH_2 emission, the precursor species would have a distributed source with a spatial profile similar to that seen for NH_2.

According to laboratory studies (e.g., Loomis et al. 2000; Woodbridge et al. 1991; Biesner et al. 1988, 1989), NH_3 is photodissociated into NH_2 in the electronic ground state ($\tilde{X}$) or in the first excited state ($\tilde{A}$). Most NH_2 radicals are formed without vibrational excitation, but with substantial rotational excitation about the a-inertial axis (and with little excitation about the other axes). Some NH_2 radicals are formed

vibrationally excited in ν_2-bending modes, however, we could not find any literature describing the fraction of NH_2 radicals that could be excited vibrationally in the ν_1- or ν_3-modes by photolysis of NH_3.

As discussed in Section 4.1, the strength of the emission line at 3181.5 cm^{-1} (4_{13}–4_{22} in the NH_2 ν_1 band) cannot be explained by our NH_2 emission model. This fact may indicate that this line was enhanced by prompt emission. Unfortunately, we could not check the spatial profile of the line due to its poor signal-to-noise ratio (S/N), and we cannot discuss this hypothesis in detail. Except for this line, we could not find any emission lines whose upper level is associated with high-K_a or high-J values. Their scarceness suggests that few NH_2 radicals are excited to the ν_1- or ν_3-vibrational modes by photodissociation of NH_3 (the emission line at 3181.5 cm^{-1} might be contaminated by an unidentified line not associated with NH_2).

4.5. Comparison of This Work with Previous Results

Ammonia abundance ratios relative to water have been reported for many comets. The in situ measurement (mass spectroscopy) in comet Halley showed NH_3/H_2O = 1.5 (+0.5/−0.7)% (Meier et al. 1994). Earlier direct (radio) measurements of ammonia provided NH_3/H_2O ratios of 0.5%–0.6% in comets Hyakutake and Hale-Bopp (Bird et al. 1997; Hirota et al. 1999). The abundance ratios were also determined in comets C/2001 Q4 (NEAT) and C/2002 T7 (LINEAR) by submillimeter observations with the *Odin* satellite. The NH_3/H_2O ratios are 0.50% ± 0.09% and 0.33% ± 0.08%, respectively (Biver et al. 2007). Near 3 μm in wavelength, direct measurements of ammonia were reported by Bonev et al. (2009), Magee-Sauer et al. (2002, 2006, 2007, 2008), and Dello Russo et al. (2007, 2009a, 2009b). The NH_3/H_2O ratios are 1.47% ± 0.27% (for T_{rot} = 150 K) and 0.52% ± 0.15% in comets C/2006 (McNaught) and 6P/d'Arrest, respectively (Dello Russo et al. 2009a, 2009b). The abundance ratio was also determined as 0.30%–0.37% in comet C/Machholz (Bonev et al. 2009), and we compare our result with their values later. Furthermore, indirect determinations of NH_3/H_2O ratios in comets have been performed in the optical wavelength region. Kawakita & Watanabe (2002) showed ammonia abundance ratios in the range 0.1%–1.5% (typically 0.5%) for the comets sampled by Fink & Hicks (1996) and based on their NH_2 measurements. Those values are consistent with the results derived by direct measurements of ammonia in some comets. In summary, the ratio of NH_3/H_2O in a comet is usually within the range from 0.1% to 1.5%. The NH_3/H_2O ratio (0.46% ± 0.03%) obtained from our study of C/Machholz falls well within this range.

C/Machholz was also observed on 2004 November 28 and 2005 January 19 by Bonev et al. (2009), who reported an upper limit (3σ) of < 0.47% for the mixing ratio of ammonia on November 28. They detected two lines of NH_3 on 2005 January 19 and derived production rates for NH_3 by adopting the rotational temperatures obtained for H_2O (93 ± 2 K), and also for HCN (76 ± 2 K). Their mixing ratios are 0.37% ± 0.06% and 0.30% ± 0.04%, respectively. Their value of 93 K agrees with our value (0.46% ± 0.03%) within errors but taken together, their results are slightly lower than ours. This discrepancy may arise from the different values used for g-factors of ammonia (probably due to the difference in solar spectrum used in the models). The g-factors of ammonia used in Bonev et al. (2009) were different from our g-factors at the same rotational temperatures (B. P. Bonev 2009, private communication), and the NH_3/H_2O ratios reported by Bonev et al. (2009) and in this work are consistent with each other if we use the same fluorescence excitation model.

5. CONCLUSION

In this paper, we present fluorescence excitation models for ammonia and NH_2 in comets. We provide quantitative g-factors (line by line) for four values of rotational temperature in the range typical of cometary comae, and we present values for a comet at perihelion at 1 AU (see the online version of Table 4). We then applied our models to spectra of C/2004 Q2 (Machholz), and derived the mixing ratio of ammonia relative to water (H_2O was measured simultaneously, and its production rate was reported by Kawakita & Kobayashi 2009). The ammonia to water ratio determined from the direct measurement of NH_3 (ν_1 band) is 0.46% ± 0.03%, comfortably within the (wide) range of values found for ammonia in other comets. We also report the mixing ratio of ammonia (0.31%–0.79%) derived from detected lines of NH_2 (ν_1 band), which is consistent with the result from direct measurement of NH_3. At the present level of accuracy, we confirm that NH_3 could be the sole parent of NH_2. With modest improvements in S/N, the simultaneous measurement of near infrared emission lines of NH_2 and NH_3 will provide an important method for testing the presence of potential progenitors of NH_2 other than ammonia.

Data presented herein were obtained at the W. M. Keck Observatory. This work was financially supported by MEXT under Grant-in-Aid for Scientific Research 22540257 (H.K.) and by the NASA Planetary Astronomy Program under RTOP 196-41-54 (M.J.M.). The authors would like to thank Hitomi Kobayashi for her great effort on the data reduction.

REFERENCES

Allen, M., Delitsky, M., Huntress, W., Yung, Y., & Ip, W.-H. 1987, A&A, 187, 502
Biesner, J., Schnieder, L., Ahlers, G., Xie, X., & Welge, K. H. 1989, J. Chem. Phys., 91, 2901
Biesner, J., Schneider, L., Schmeer, J., Ahlers, G., & Xie, X. 1988, J. Chem. Phys., 88, 3607
Bird, M. K., Hatchell, J., Van Der Tak, F. F. S., Crovisier, J., & Bockelée-Morvan, D. 2002, in Proc. Asteroids, Comets, Meteors—ACM 2002, ed. B. Warmbein (ESA SP-500; Noordwijk: ESA), 697
Bird, M. K., Huchtmeier, W. K., Gensheimer, P., Wilson, T. L., Janardhan, P., & Lemme, C. 1997, A&A, 325, L5
Biver, N., et al. 2007, Planet. Space Sci., 55, 1058
Bonev, B. P., & Mumma, M. J. 2006, ApJ, 653, 788
Bonev, B. P., Mumma, M. J., Dello Russo, N., Gibb, E. L., DiSanti, M. A., & Magee-Sauer, K. 2004, ApJ, 615, 1048
Bonev, B. P., Mumma, M. J., DiSanti, M. A., Dello Russo, N., Magee-Sauer, K., Ellis, R. S., & Stark, D. P. 2006, ApJ, 653, 774
Bonev, B. P., Mumma, M. J., Gibb, E. L., DiSanti, M. A., Villanueva, G. L., Magee-Sauer, K., & Ellis, R. S. 2009, ApJ, 699, 1563
Burkholder, J. B., Howard, C. J., & McKellar, A. R. W. 1988, J. Mol. Spectrosc., 127, 415
Dello Russo, N., Mumma, M. J., DiSanti, M. A., Magee-Sauer, K., Gibb, E. L., Bonev, B. P., McLean, I. S., & Xu, L.-H. 2006, Icarus, 184, 255
Dello Russo, N., Vervack, R. J., Jr., Weaver, H. A., Biver, N., Bockelée-Morvan, D., Crovisier, J., & Lisse, C. M. 2007, Nature, 448, 172
Dello Russo, N., Vervack, R. J., Jr., Weaver, H. A., Kawakita, H., Kobayashi, H., Biver, N., Bockelée-Morvan, D., & Crovisier, J. 2009a, ApJ, 703, 187
Dello Russo, N., Vervack, R. J., Jr., Weaver, H. A., & Lisse, C. M. 2009b, Icarus, 200, 271
Dello Russo, N., Vervack, R. J., Jr., Weaver, H. A., Montgomery, M. M., Deshpande, R., Fernández, Y. R., & Martin, E. L. 2008, ApJ, 680, 793
DiSanti, M. A., & Mumma, M. J. 2008, Space. Sci. Rev., 138, 127
Dressler, K., & Ramsay, D. A. 1959, Phil. Trans. R. Soc. A, 251, 553

Feldman, P., Cochran, A., & Combi, M. 2004, in COMET II, ed. M. Festou, H. U. Keller, & H. A. Weaver (Tucson, AZ: Univ. Arizona Press), 425
Fink, U., & Hicks, M. D. 1996, ApJ, 459, 729
Hase, F., Wallace, L., McLeod, S. D., Harrison, J. J., & Bernath, P. F. 2010, J. Quant. Spectrosc. Radiat. Transfer, 111, 521
Haser, L. 1957, Bull. Acad. R. Sci. Liege, 43, 740
Herzberg, G. 1966, Molecular Spectra and Molecular Structure, Vol. 3 (New York: Van Nostrand), 104
Hirota, T., Yamamoto, S., Kawaguchi, K., Sakamoto, A., & Ukita, N. 1999, ApJ, 520, 895
Huebner, W., Keady, J. J., & Lyon, S. P. 1992, Astrophys. Space Sci., 195, 1
Jackson, W. M. 1976a, J. Photochem., 5, 107
Jackson, W. M. 1976b, in Proc. IAU Colloq. 25, The Study of Comets, ed. B. Donn, M. Mumma, W. Jackson, M. A'Hearn, & R. Harrington, 679
Jensen, P., Kraemer, W. P., & Bunker, P. R. 2003, Mol. Phys., 101, 613
Kawakita, H., Jehin, E., Manfroid, J., & Hutsemékers, D. 2007, Icarus, 187, 272
Kawakita, H., & Kobayashi, H. 2009, ApJ, 693, 388
Kawakita, H., & Watanabe, J. 1998, ApJ, 495, 946
Kawakita, H., & Watanabe, J. 2002, ApJ, 572, L77
Kawakita, H., Watanabe, J., Furusho, R., Fuse, T., Capria, M. T., De Sanctis, M. C., & Gabriele, C. 2004, ApJ, 601, 1152
Kawakita, H., Watanabe, J., Fuse, T., Furusho, R., & Abe, S. 2002, Earth Moon Planets, 90, 371
Kawakita, H., et al. 2001, Science, 294, 1089
Kawakita, H., et al. 2006, ApJ, 634, 1337
Kleiner, I., Brown, L. R., Tarrago, G., Kou, Q.-L., Picqué, N., Guelachvili, G., Dana, V., & Mandin, J.-Y. 1999, J. Mol. Spectrosc., 193, 46
Kobayashi, H., & Kawakita, H. 2009, ApJ, 703, 121
Kobayashi, H., Kawakita, H., Mumma, M. J., Bonev, B. P., Watanabe, J., & Fuse, T. 2007, ApJ, 668, L75
Krasnopolsky, V., & Tkachuk, A. 1991, AJ, 101, 1915
Kurucz, R. L. 1994, in Proc. 154th Symposium of the International Astronomical Union, Infrared Solar Physics, ed. D. M. Rabin, J. T. Jefferies, & C. Lindsey (Dordrecht: Kluwer), 523
Kurucz, R. L. 2005, Mem. Soc. Astron. Ital. Suppl., 8, 189
Loomis, R. A., Reid, J. P., & Leone, S. R. 2000, J. Chem. Phys., 112, 658
Magee-Sauer, K., Dello Russo, N., DiSanti, M. A., Gibb, E. L., & Mumma, M. J. 2002, in Proc. Asteroids, Comets, Meteors—ACM 2002, ed. B. Warmbein (ESA SP-500; Noordwijk: ESA), 549
Magee-Sauer, K., Feuss, J. W., Dello Russo, N., DiSanti, M. A., Bonev, B. P., Gibb, E. L., Villanueva, G. L., Anderson, W. M., & Mumma, M. J. 2006, BAAS, 38, 534
Magee-Sauer, K., Mumma, M. J., Bonev, B. P., Radeva, Y. L., DiSanti, M. A., Villanueva, G. L., Dello Russo, N., Gibb, E. L., & Anderson, W. M. 2007, BAAS, 39, 523
Magee-Sauer, K., Villanueva, G. L., Mumma, M. J., Bonev, B. P., DiSanti, M. A., Dello Russo, N., Lippi, M., & Gibb, E. L. 2008, BAAS, 40, 415
McKellar, A. R. W., Vervloet, M., Burkholder, J. B., & Howard, C. J. 1990, J. Mol. Spectrosc., 142, 319
McLean, I. S., et al. 1998, Proc. SPIE, 3354, 566
Meier, R., Eberhardt, P., Krankowsky, D., & Hodges, R. R. 1994, A&A, 287, 268
Müller, H. S. P., Klein, H., Belov, S. P., Winnerwisser, G., Morino, I., Yamada, K. M. T., & Saito, S. 1999, J. Mol. Spectrosc., 195, 177
Mumma, M. J., et al. 2001, ApJ, 546, 1183
Oka, T. 1968, J. Chem. Phys., 49, 3135
Palmer, P., Wootten, A., Butler, B., Bockelée-Morvan, D., Crovisier, J., Despois, D., & Yeomans, D. K. 1996, BAAS, 28, 927
Pine, A. S., & Dang-Nhu, M. 1993, J. Quant. Spectrosc. Radiat. Transfer, 50, 565
Ross, S. C., Birss, F. W., Vervloet, M., & Ramsay, D. A. 1988, J. Mol. Spectrosc., 129, 436
Rothman, L. S., et al. 2005, J. Quant. Spectrosc. Radiat. Transfer, 96, 13
Rothman, L. S., et al. 2009, J. Quant. Spectrosc. Radiat. Transfer, 110, 533
Šimečková, M., Jacquemart, D., Rothman, L. S., Gamache, R. R., & Goldman, A. 2006, J. Quant. Spectrosc. Radiat. Transfer, 98, 130
Tegler, S., & Wyckoff, S. 1989, ApJ, 343, 445
Weaver, H. A., & Mumma, M. J. 1984, ApJ, 278, 782
Woodbridge, E. L., Ashfold, M. N. R., & Leone, S. R. 1991, J. Chem. Phys., 94, 4195
Xie, X., & Mumma, M. J. 1992, ApJ, 386, 720